Slow Switching in Globally Coupled Oscillators

Hiroshi Kori

Department of Physics, Graduate School of Sciences,
Kyoto University, Kyoto 606-8502, Japan

Thesis submitted for admission to the doctor's degree,
Kyoto University, January 2002

Abstract

Slow switching phenomenon in globally coupled oscillators is discussed. The phenomenon appears as a result of approach of the system to heteroclinic loops. A particular stability property of two-cluster states and a certain symmetry of our model are responsible for the formation of the heteroclinic loop. The resulting heteroclinic loop is stably formed through invariant subspaces that exist for the certain symmetry of our model, and it is robust under small perturbation unless the symmetry is broken. The physical mechanism of the formation of the heteroclinic loop does not depend on the structure of elements and the origin of coupling. The phenomenon actually arises in a wide class of coupled oscillator system. The heteroclinic loop is easily formed near the bifurcation point where the state of perfect synchrony loses stability. By the analysis near the bifurcation point, it is argued that the local stability conditions for the formation of an attracting heteroclinic loop are generally satisfied just above the bifurcation point. Such bifurcation can be induced by time delay in coupling. We assume weak coupling in theoretical approaches, which provides considerable advantages in analytic study of the system.

Contents

Chapter 1

General Introduction

Studies on collective motion of coupled oscillators have attracted considerable attention over the last few decades. One of the strong driving force behind the study would be an interest in biological rhythms [1,2]. It is commonly seen that a population of autonomous elements behaves collectively and make a macroscopic rhythm, such as heartbeats [3], flashing fireflies [4], synchronous sugar metabolism of yeast cells [5]. Such macroscopic rhythms are formed when not only frequency but also *phase* of elements are synchronized. Many significant results about such synchronization have been obtained by studying globally coupled oscillators, i.e., a population of oscillators coupled through a mean-field (see Refs. [6–8]; Chaps. 4 and 12 in Ref. [9]; and references therein). One may think global coupling is unrealistic. However, there actually exist systems with global coupling, such as spatially extended chemical oscillators coupled via optics or gas, Josephson junction arrays, and multimode lasers. Besides, there could be certain cases that the global coupling is an appropriate approximation of long range interactions in biology, such as flushing fireflies, yeast cells communicating via a common medium, and the network of neurons.

A system with globally coupled oscillators, in spite of its simple form of dynamical equations, shows rich behavior even if all the oscillators are identical, i.e., obey the same dynamical equations. One of the remarkable discovery there would be that identical dynamical elements do not necessarily behave identically. K. Okuda has shown that identical oscillators can form several clusters each of which is perfectly phase-synchronized [10]. It is interesting that a population of identical elements causes a spontaneous phase separation. Recently, such a clustering phenomenon has actually been reported experimentally in spatially extended chemical oscillators coupled globally [11,12].

There is a peculiar type of clustering phenomenon, which has first been studied by D. Hansel *et al.* in a particular class of globally coupled phase oscillators [13]. They showed numerically that the system slowly switches back and forth among pairs of two-cluster states, and each switching is accompanied by intriguing collective dynamics. This

phenomenon is called *slow switching*. The slow switching phenomenon was interpreted in terms of the formation of a heteroclinic loop between the pair of two-cluster states, which was supported by all numerical results presented there (see Chap. 2 for details). Although their findings are important, explanation is still needed as to why the heteroclinic loop arises inevitably and persists robustly against our common belief in its structural instability.

The present thesis is organized as follows. We briefly review the work of D. Hansel *et al.* studied in Ref. [13] in Chap. 2 for an introduction of the slow switching phenomenon. In Chap. 3, we show and discuss the phenomenon in a network of neural oscillators. By considering the stability of cluster states and symmetry possessed by the model, we argue that a heteroclinic loop between a pair of two-cluster states arise inevitably and persists robustly in the system. The physical mechanism we describe there does not depend on the nature of elements (phase oscillator, limit cycle oscillator, excitable elements, chaotic elements, etc.) and the origin of couplings (diffusive coupling, pulse coupling, delayed coupling, etc.). The slow switching phenomenon actually arises in various classes of coupled oscillator models, which is demonstrated in Chap. 4. We also argue there that the heteroclinic loop is easily formed near the bifurcation point where the state of perfect synchrony loses stability. Such bifurcation can be induced by time delay in coupling.

Chapter 2

The Slow Switching Phenomenon

The content of this chapter is a brief review of Ref. [13]

2.1 Slow switching in the phase model

The population model we consider in this chapter consists of N identical phase oscillators with global coupling, given by

$$\frac{d}{dt}\psi_i(t) = \omega + \frac{K}{N}\sum_{j=1}^{N}\Gamma(\psi_i - \psi_j), \tag{2.1}$$

where ψ_i $(0 \leq \psi_i < 2\pi)$ is the phase of the i-th oscillator $(i = 1, 2, \cdots, N)$, $\Gamma(x)$ is the *coupling function* with 2π periodicity, ω is arbitrary constant denoting the intrinsic frequency of each oscillator, and K is arbitrary positive constant denoting the coupling strength.

We assume the following particular coupling function:

$$\Gamma(x) = -\sin(x + 1.25) + 0.25\sin(2x). \tag{2.2}$$

Numerically integrating the above model under initial conditions, we generally observe *slow switching phenomenon* provided $N \geq 4$. The collective behavior of the system can conveniently be described in terms of the order parameter defined by

$$O(t) = \frac{1}{N}\left|\sum_{j=1}^{N}\exp[i\psi_j]\right|. \tag{2.3}$$

Its value is 1 for perfect synchrony and 0 for unform distribution of the phases. A time trace of the order parameter is displayed in Fig. 2.1. We can see undulation of the order parameter for a long time after which the parameter converges to a nontrivial value constant in time, implying that the system converges to a certain collective state rotating steadily. Peculiar dynamics is observed until the convergence. As exhibited in Fig. 2.2, the whole population, which is initially distributed almost uniformly, splits into two subpopulations, each of which converges almost to a point cluster. After some time, however, this seeming convergence turns out to be unstable, and the phase-advanced cluster starts to scatter. Then, after some time, a group of the scattered oscillators converges again as it comes behind the preexisting cluster. In this way, the preexisting cluster becomes a phase-advanced cluster. After some time, again, this phase-advanced cluster begins to scatter, and a similar process repeats again and again. In other words, the system switches back and forth between a pair of two-cluster states. The time interval during which the system is trapped near two-cluster states increases exponentially with time. At a certain time, however, the system converges to one of the two-cluster states and stops switching.

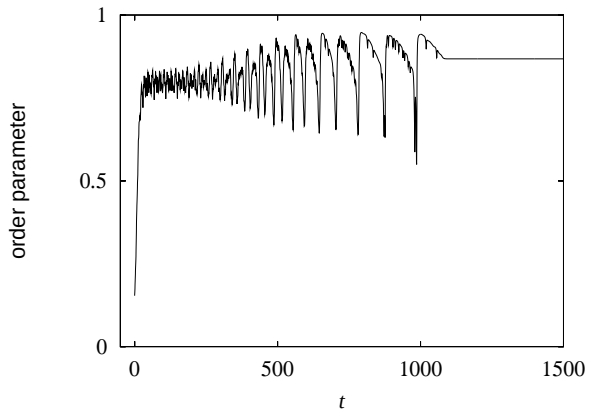

Figure 2.1: A time trace of the order parameter. The system converges to a steadily rotating two-cluster state after a long transient. The parameter values are $K = 1$ and $N = 100$. The order parameter is irrelevant to the value of ω.

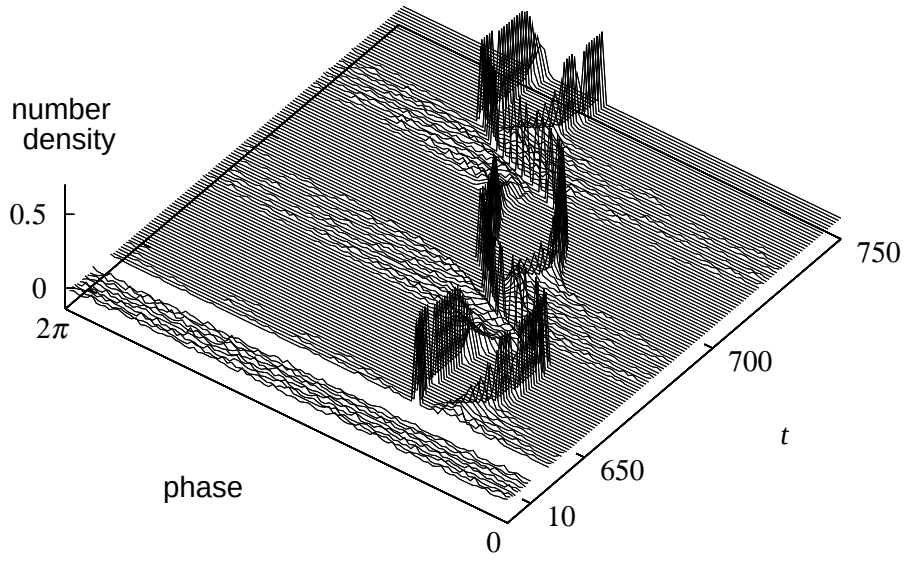

Figure 2.2: Slow switching phenomenon viewed through the number density of the oscillators as a function of the phase. The parameter values are $\omega = 0.79$, $K = 1$, and $N = 100$.

2.2 Stability analysis of two-cluster states and the heteroclinic loop

We study the existence and stability of a two-cluster state in which the two clusters consist of Np and $N(1-p)$ oscillators. The oscillators inside each cluster are completely phase-synchronized. The phase difference of the two clusters denoted by Δ is constant in time, and the clusters rotate at a constant frequency. Such a steadily rotating two-cluster state can be denoted by (p, Δ). In a two-cluster state, the phase difference Δ obeys from Eq. (2.1)

$$\frac{d}{dt}\Delta = K\{(2p-1)\Gamma(0) + (1-p)\Gamma(\Delta) - p\Gamma(-\Delta)\}. \tag{2.4}$$

Since Δ is constant in a steadily rotating two-cluster states, we obtain the relation between p and Δ, given by

$$p = \frac{\Gamma(0) - \Gamma(\Delta)}{2\Gamma(0) - \Gamma(\Delta) - \Gamma(-\Delta)}. \tag{2.5}$$

Various (p, Δ) exist with different sets of p and Δ.

We then study the stability of the two-cluster states. Calculation of stability matrix is rather complicated but straightforward. Eigenvalues of the stability matrix are

$$\lambda_0 = 0, \tag{2.6}$$

$$\lambda_1 = K\{p\Gamma'(0) + (1-p)\Gamma'(\Delta)\}, \tag{2.7}$$

$$\lambda_2 = K\{(1-p)\Gamma'(0) + p\Gamma'(-\Delta)\}, \tag{2.8}$$

$$\lambda_3 = K\{(1-p)\Gamma'(\Delta) + p\Gamma'(-\Delta)\}, \tag{2.9}$$

where $\Gamma'(x)$ means $(d/dx)\Gamma(x)$. The multiplicity of λ_i $(i = 0, 1, 2, 3)$ are 1, $Np-1$, $N(1-p)-1$ and 1, respectively. λ_0 vanishes identically because of the invariance of Eq. (3.18) with respect to an identical shift of all the phases. λ_1 and λ_2 correspond to fluctuations in phase of the two oscillators inside the phase-advanced and phase-retarded cluster, respectively. λ_3 corresponds to a fluctuation in Δ.

Substituting Eq. (2.2) into Eq. (2.5), we obtain the relation between p and Δ, shown in Fig. 2.3(a). By using the relation, the eigenvalues of (p, Δ) can be calculated, which is displayed in Fig. 2.3(b). We find that all of the two-cluster states to which the system *converges* are linearly unstable. The seeming contradiction here, however, can be interpreted in terms of the formation of heteroclinic loops between pairs of the two-cluster states. We denote such a pair by (p, Δ) and (p, Δ') with $\Delta > 0$ and $\Delta' < 0$. Under the assumption

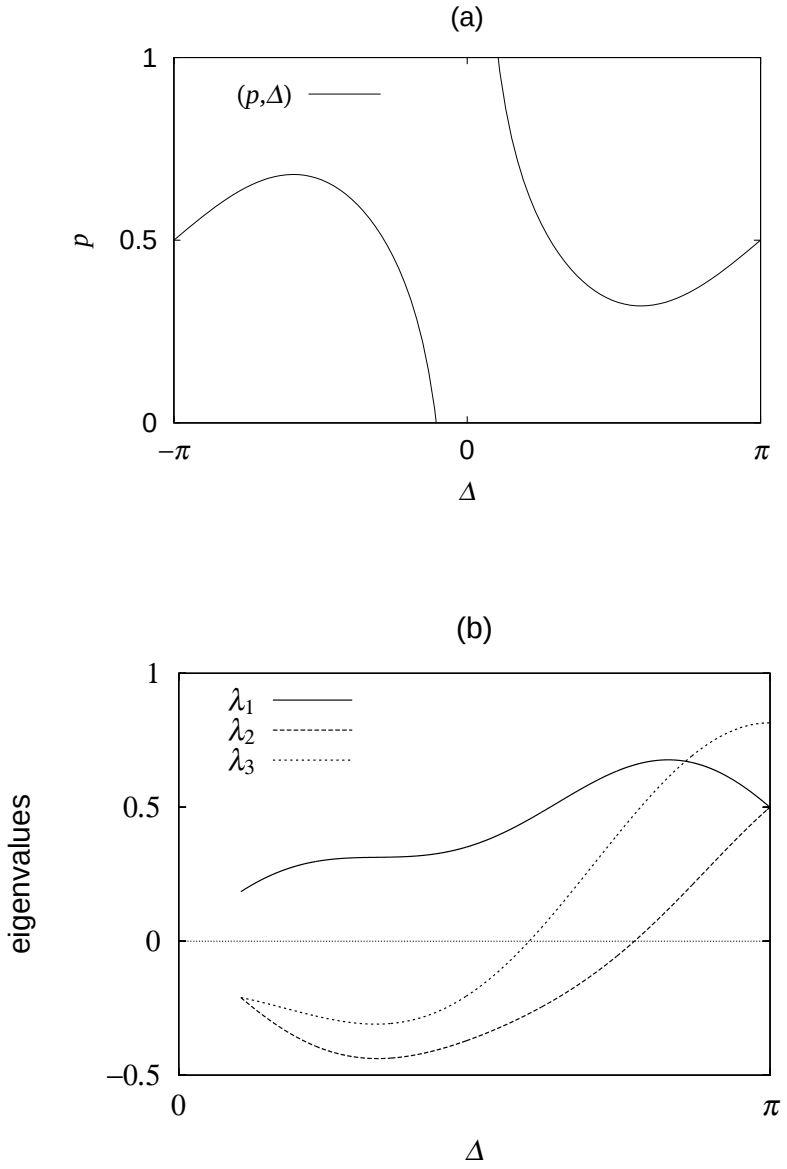

Figure 2.3: The existence and stability condition of the two-cluster states. (a)The relation between p and Δ in the two-cluster state. (b)The eigenvalues of the two-cluster state plotted as a function of Δ.

of the existence of a heteroclinic loop between (p, Δ) and (p, Δ'), one can verify that the heteroclinic loop is *attracting* if

$$\gamma \equiv \frac{\lambda_2 \lambda_1'}{\lambda_1 \lambda_2'} > 1, \tag{2.10}$$

where λ_i and λ_i' $(i = 1, 2)$ are the eigenvalues of (p, Δ) and (p, Δ'), respectively. In that case, a trajectory moves along the heteroclinic loop and comes to be closer to these fixed points. After $2n$ switching (i.e., n cycles), the time spent around the fixed point and the distance to it will be

$$T_n \sim T_0 \gamma^n, \tag{2.11}$$

$$\epsilon_n \sim \epsilon_0^{\gamma^n}. \tag{2.12}$$

In numerical integrations, ϵ_n goes to zero in a finite time due to the round-off error, so that the system converges to one of the fixed point.

2.3 Dynamics under small noise

When the system is disturbed by small noise, switching between a pair of two-cluster states occurs almost periodically. To demonstrate it, we generalize the model as follows:

$$\frac{d}{dt}\psi_i(t) = \omega + \frac{K}{N}\sum_{j=1}^{N} \Gamma(\psi_i - \psi_j) + \sigma \xi_i(t), \tag{2.13}$$

where $\xi_i(t)$ is a Gaussian white noise with the variance 1, and σ is a constant denoting the intensity of the noise. The coupling function Γ is given by Eq. (2.2) here also. Figure 2.4 displays a time trace of the order parameter for the noisy system. The flat and descendent parts of the order parameter respectively indicate the periods in which each cluster is almost a point cluster and one of the clusters is scattering. For such a noisy system, the time it take for the system to perform a cycle of switching is estimated at

$$T \sim -\left(\frac{1}{\lambda_1} + \frac{1}{\lambda_2'}\right) \ln \sigma. \tag{2.14}$$

The value of the slope obtined is in good agreement with the slope obtained from Fig. 2.5.

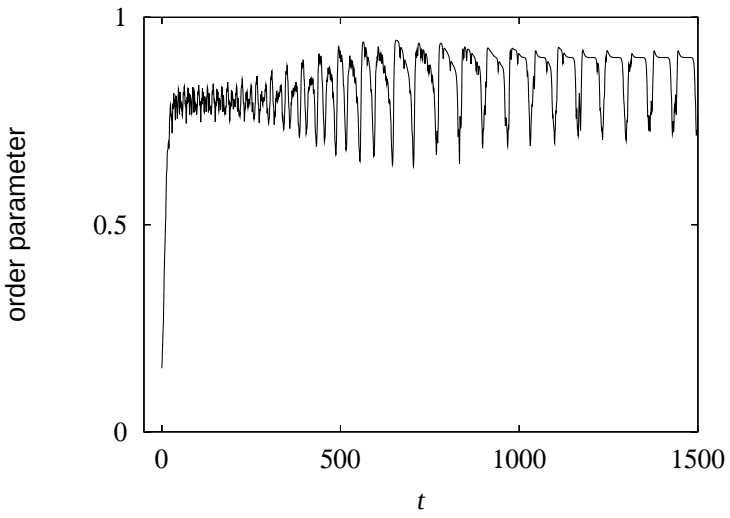

Figure 2.4: A time trace of the order parameter under weak noise ($\mu = 10^{-8}$).

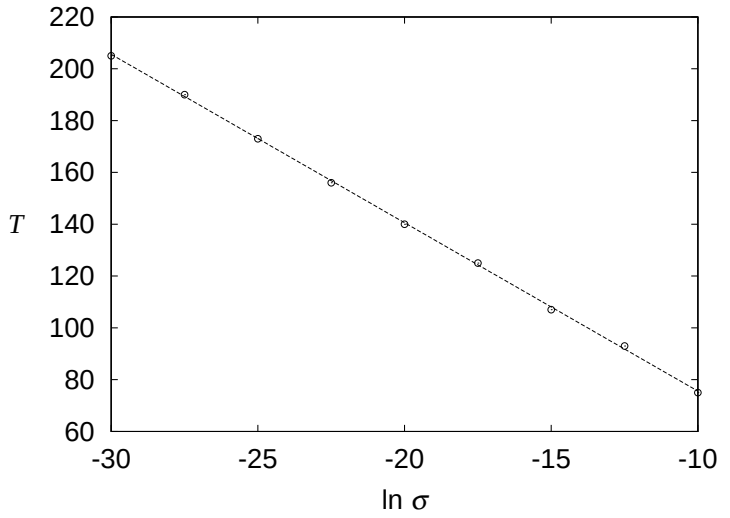

Figure 2.5: Period T of a cycle versus $\ln \sigma$. The line is a linear fitting of the date.

Chapter 3

Leaky Integrate-and-Fire Oscillators with Delayed Pulse-Coupling

3.1 Introduction

It has been pointed out that collective motion of neurons in the brain is crucial to information processing and transmission (see, e.g. Ref. [14]). In the brain, the neurons are exclusively coupled through chemical synapses, i.e., the neurons communicate by pulses of transmitter [15]. Chemical synapses commonly form dense and complex networks. For mathematical modeling of neuronal networks, homogeneous all-to-all (i.e. global) coupling is often adopted. Although the global coupling may be a little too idealistic, the corresponding networks share a lot of properties in common with systems with complex and dense networks.

In this chapter, we consider a population of neural oscillators with delayed, all-to-all pulse-coupling. The oscillator we use is called the leaky integrate-and-fire (LIF) model. There are a large amount of papers concerning LIF in physics and neuroscience, e.g. see [16–18]. This is because LIF is a quite simple model, still it captures some essential characteristics of neuronal dynamics, i.e., it represents an integrator with relaxation, and resets after it fires. Although our population model is commonly used, (see, e.g. [19]), its collective dynamics does not seem to have been studied so carefully. We will show that various kind of cluster states arise in our model, and discuss the slow switching phenomenon in particular.

3.2 Model

The population model we consider consists of N identical elements with delayed, all-to-all pulse-coupling. The dynamics of each elements is described by a single variable v_i $(i = 1, 2, \ldots, N)$ which corresponds to the membrane potential of a neuron. The equation for v_i is given by

$$\frac{d}{dt}v_i(t) = a - v_i + \frac{K}{N}(b - v_i)E(t). \tag{3.1}$$

The parameter a is the so-called resting potential to which v_i relaxes when the coupling is absent. It is assumed that when v_i reaches a threshold value which is set to 1, it is instantaneously reset to zero. This event is interpreted as a spiking, or firing, event. The dynamics is thus called LIF. When a neuron spikes, it emits a pulse toward each neuron coupled to it, and the latter receives the pulse with some delay called a synaptic delay. The coupling is assumed to be homogeneous and all-to-all, so that its effect can be represented by one global variable E, given by

$$E(t) = \sum_{j=1}^{N} \sum_{\text{spikes}} e(t - t_j^{\text{spikes}} - \tau). \tag{3.2}$$

Here, t_j^{spikes} represents a series of times at which the j-th neuron spikes and $\sum_{\text{spikes}}$ denotes a summation over the series of such spikes; τ is the synaptic delay, and $e(t)$ is a *pulse function*, given by

$$e(t) = \frac{\alpha\beta}{\beta - \alpha}(e^{-\alpha t} - e^{-\beta t})\Theta(t), \tag{3.3}$$

where $\Theta(t)$ is the Heaviside function; α and β are constants satisfying $\beta > \alpha$. α^{-1} and β^{-1} give characteristic time scales of the pulse function. In the limit $\beta \to \alpha$, $e(t)$ becomes $\alpha^2 t e^{-\alpha t}$, which is called the alpha function [15]. b is called the reversal potential to which v_i relaxes when $E(t)$ is positive, i.e. while the neuron receives the pulses. K is a positive constant characterizing the strength of the coupling. The coupling assumed above is characteristic to the synaptic coupling. The coupling becomes excitatory (EPSP) if $b > 1$, and inhibitory (IPSP) if $b \leq 0$.

If $a \leq 1$, LIF becomes an excitable neuron, while if $a > 1$, it repeats periodic spikings, namely, it represents a neural oscillator. We assume $a > 1$ hereafter. Then, we can define a variable varying smoothly with time, which turns out useful in the following discussion. We definethe *phase* of the i-th neuron as

$$\psi_i = \int_0^{v_i} \frac{dv}{a - v} = \ln\left(\frac{a}{a - v_i}\right). \tag{3.4}$$

which varies between 0 and the intrinsic period of oscillation T, given by

$$T = \ln\left(\frac{a}{a - 1}\right). \tag{3.5}$$

Note that ψ_i satisfies $d\psi_i/dt = 1$ in the absence of coupling.

3.3 Numerical results

By numerically integrating our model under random distribution of v_i, we find various types of collective behavior. Among them, we are particularly interested in the slow switching phenomenon, which actually occurs when $b > a$ and $N \geq 4$ (see Chap. 2 for the explanation of the phenomenon).

The slow switching phenomenon occurs within a broad range of parameter values provided that K is small and the time constants α^{-1}, β^{-1} and τ are small compared with T. For larger α^{-1}, β^{-1} and τ, the slow switching phenomenon becomes less probable, and the appearance of steady multi-cluster states becomes more probable instead. For $b < a$, we find no two-cluster states involving slow switching, while steady multi-cluster states are observed in most cases. A detailed phase diagram will be presented in §3.7.

3.4 Weak coupling limit

Our model given by Eq. (3.1) is relatively simple, still it is not easy to get some insight into its collective dynamics analytically. Fortunately, however, our main results given in §3.3 do not change qualitatively in the weak coupling limit, i.e. $K \to 0$. In this limit, our model is reduced to a much simpler form with which we can study the existence and stability of various cluster states analytically. Derivation of the reduced model is given as follows.

Substituting $v_i = a(1 - e^{-\psi_i})$ into Eq. (3.1), we obtain

$$\frac{d}{dt}\psi_i(t) = 1 + \frac{K}{N}\sum_{j=1}^{N}\sum_{\text{spikes}} Z(\psi_i)e(t - t_j^{\text{spikes}} - \tau), \tag{3.6}$$

where

$$Z(\psi_i) = \frac{b-a}{a}e^{\psi_i} + 1. \tag{3.7}$$

It is convenient in the following calculation to redefine Z as a T-periodic function, i.e. $Z(\psi_i + nT) = Z(\psi_i)$ $(n = \pm 1, \pm 2, \cdots)$. Note that sudden drop of $Z(\psi_i)$ at $\psi_i = 0$ is due to the rule employed in our model, i.e., the membrane potential is reset instantaneously at $v_i = 0$. We also define a residual phase Ψ_i by

$$\Psi_i = \psi_i - t. \tag{3.8}$$

Substituting Eq. (3.8) into Eq. (3.6), we obtain

$$\frac{d}{dt}\Psi_i(t) = \frac{K}{N}\sum_{j=1}^{N}\sum_{\text{spikes}} Z(\Psi_i + t)e(t - t_j^{\text{spikes}} - \tau). \tag{3.9}$$

We now assume that K is sufficiently small so that the r.h.s of Eq. (3.9) is sufficiently smaller than the intrinsic frequency T^{-1}. This allow us to make averaging of the r.h.s of Eq. (3.9) over the period T. The zeroth order approximation with respect to the smallness of K, which corresponds to the free oscillations of the oscillators, is given by

$$\Psi_i(t) = \text{const.} \tag{3.10}$$

and

$$t_j^{\text{spikes}} = t_j - nT, \quad (n = 0, 1, 2, \ldots), \tag{3.11}$$

where t_j is the latest time at which the j-th neuron spikes. In the first order approximation, we may time-average Eq. (3.9) over the range between $t - T$ and t using Eqs. (3.10) and

(3.11):

$$\frac{d}{dt}\Psi_i(t) = \frac{K}{N}\sum_{j=1}^{N}\frac{1}{T}\int_{t-T}^{t}\sum_{n=0}^{\infty} Z(\Psi_i(t)+\lambda)e(\lambda - t_j + nT - \tau)d\lambda \tag{3.12}$$

$$= \frac{K}{N}\sum_{j=1}^{N}\frac{1}{T}\int_{0}^{\infty} Z(\Psi_i(t)+t_j+\tau+\lambda')e(\lambda')d\lambda' \tag{3.13}$$

$$= \frac{K}{T} + \frac{K(b-a)}{Na}\sum_{j=1}^{N}\Gamma\big(\Psi_i(t)+t_j+\tau\big), \tag{3.14}$$

where

$$\Gamma(x) = \frac{\alpha\beta}{\beta-\alpha}\big\{H_{\alpha,T}(x) - H_{\beta,T}(x)\big\}, \tag{3.15}$$

$$H_{\alpha,T}(x) = \frac{1}{T}\int_0^\infty \exp[(x+\lambda) \bmod T]\exp[-\alpha\lambda]d\lambda$$

$$= \frac{(e^T-1)\exp[\alpha(x \bmod T)] - (e^{\alpha T}-1)\exp[x \bmod T]}{T(1-\alpha)(e^{\alpha T}-1)}. \tag{3.16}$$

Note that $\Gamma(x)$ is a T-periodic function. Figure 3.1 illustrates a typical shape of the coupling function given by Eq. (3.15). Furthermore, using the identity

$$\Psi_j(t_j) = \psi_j(t_j) - t_j = -t_j, \tag{3.17}$$

and the zeroth order approximation $\Psi_j(t_j) = \Psi_j(t)$, we may replace t_j by $-\Psi_j(t)$ in Eq. (3.14) in the first order approximation. Thus, we finally obtain

$$\frac{d}{dt}\psi_i(t) = \omega + \frac{K'}{N}\sum_{j=1}^{N}\Gamma\big(\psi_i(t) - \psi_j(t) + \tau\big), \tag{3.18}$$

where $\omega = 1 + K/T$ and $K' = K(b-a)/a$. Equation (3.18) is the standard form of the phase model. Note that the error involved in Eq. (3.11) may look to diverge as $n \to \infty$, still the final error vanishes in the first order approximation due to the decay of $e(t)$. It is remarkable that the reduced model is free from memory effects, and the effect of delay has been simply converted to a phase shift in the coupling function. As shown in §4.4, similar form of the phase model is generally obtained in delayed coupled oscillators when the coupling is sufficiently weak.

The phase model given in Eq. (3.18) is invariant under a constant phase shift of all the phases, so that the dynamics of the mean phase (i.e., the center of mass) can be decoupled. We will ignore the degree of freedom associated with this dynamics hereafter.

Important parameters of our phase model given by Eq. (3.18) with Eq. (3.15) are T, α, β, τ and the sign of K' (i.e. the sign of $b-a$). The reason is the following. We

may take $|K'| = 1$ by properly rescaling of t and ω, while its sign is crucial because the local stability of any solution depends on it. ω gives the frequency of steady rotation of the whole system, which is irrelevant to collective dynamics. T gives a characteristic time scale of our model, which can be chosen as an independent parameter by which a becomes dependent through Eq. (3.5). It is remarkable that our coupling function is independent of b. In fact, change in b causes no qualitative change in our result as far as the sign of $b - a$ remains the same. Furthermore, even if we replace the term $b - v_i$ by a constant c in Eq. (3.1), i.e.,

$$\frac{d}{dt}v_i(t) = a - v_i + \frac{Kc}{N}E(t), \tag{3.19}$$

then we can reduce this model similarly and obtain the same coupling function as in Eq.(3.15), which is a little surprising result. We have checked that Eq. (3.19) actually reproduces qualitatively the same results as those given in §3.3. In that case, negative c corresponds to the case $b < a$ in Eq. (3.1). In the following sections, we assume $b > a$ and $\beta \to \alpha$ unless stated otherwise.

3.5 Two-oscillator system

In this section, we study a two-oscillator system, i.e. $N = 2$. Although the two-oscillator system is not directly related to the main subject of the present chapter, one may learn some basic properties of our phase model from this simple case. Defining $\Delta = \psi_1 - \psi_2$, we obtain

$$\frac{d\Delta}{dt} = \frac{K'}{2}\big(\Gamma(\Delta + \tau) - \Gamma(-\Delta + \tau)\big) \equiv G_\tau(\Delta). \tag{3.20}$$

Phase locking solutions are obtained by putting $d\Delta/dt = 0$, and the associated eigenvalues are given by $dG_\tau/d\Delta$. Figure 3.2 shows a bifurcation diagram of the phase locking solutions, in which we take τ as a control parameter. We find that for small τ the trivial solutions $\Delta = 0$ (in-phase locking) and $T/2$ (anti-phase locking) are unstable, while there are a pair of stable branches of non-trivial solutions. The point $\tau = 0$ is close to the bifurcation point where the in-phase state loses stability via a subcritical pitchfork bifurcation. The bifurcation occurs at $\tau = \tau_c$, where τ_c corresponds to the minimum of $\Gamma(x)$ (see Fig. 3.1). Because τ_c is negative, the in-phase state cannot be stable for small or vanishing delays (while it can be stable for delays comparable to T due to the T-periodic nature of our phase model). The width of the stable branches of the trivial solutions is the same as that of the decreasing part of $\Gamma(x)$. Owing to the peculiar shape of $Z(x)$, the width is of the same order as the width of $e(t)$, which is $O(\alpha^{-1})$. The stability of the in-phase state is identical with that of the state of perfect synchrony.

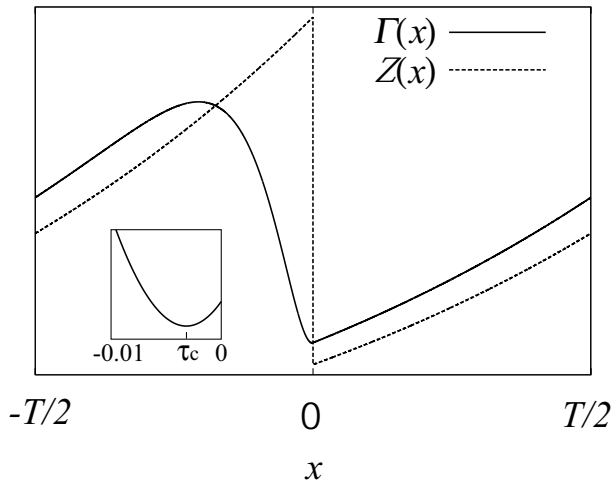

Figure 3.1: The solid line shows the coupling function $\Gamma(x)$ for $a = 1.05$ ($T \simeq 3.0$), $\alpha^{-1} = 0.2$ and $\beta \to \alpha$. The minimum appears at $x = \tau_c$ ($\simeq -0.003$) which is a small negative. For comparison, $Z(x)$ is also displayed with the broken line.

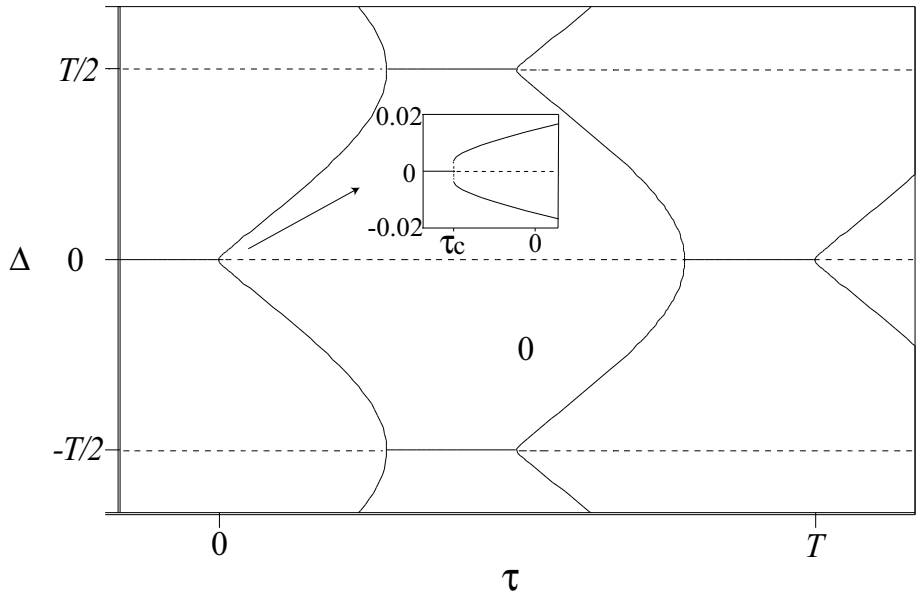

Figure 3.2: Bifurcation diagram of a two-oscillator system with the same parameter values as in Fig. 3.1. Solid and dotted lines respectively represent stable and unstable branches, where $b > a$ is assumed. The stability property is reversed when $b < a$.

In terms of the original model, we will now present a qualitative interpretation of why the in-phase locking state is unstable for small or vanishing delays. We consider the dynamics of two neurons which are initially very close in phase. The effect of a pulse on the phase ψ_i is larger for smaller dv_i/dt. dv_i/dt is monotonously decreasing except the instant it is reset (which reflects on the property of $Z(x)$ that it is increasing except $x = 0$). Thus, the neuron with larger v_i makes a larger jump in phase when it receives a pulse, by which the phase difference between the two neurons becomes larger when they receive a pulse. On the other hand, the situation becomes different if two neurons lie before and after the resetting point, i.e., if the phase-advanced neuron has smaller v_i. In that case, the phase difference becomes smaller when they receive a pulse. According to our employed rule, however, resetting and spiking occur simultaneously, so that the phase-advanced neuron almost always has larger v_i when they receive pulses. Therefore, the in-phase state becomes inevitably unstable even without delay. If we want to obtain a stable in-phase state for small or vanishing delays, we should employ a rule such that a neuron spikes before it is reset, which would be more physiologically plausible than the rule employed here.

3.6 Local stability analysis for a large population

The trivial in-phase solution and the non-trivial solutions of the two-oscillator system correspond respectively to the state of perfect synchrony and two-cluster states in the case of a large population. In this section, we study local stability of the two-cluster states. Although non-trivial solutions are stable for small delays in the two-oscillator system, the corresponding two-cluster states turn out unstable.

We consider a steadily oscillating two-cluster state in which the two clusters consist of Np and $N(1-p)$ oscillators, respectively. The oscillators inside each cluster are completely phase-synchronized, and the phase-difference between the clusters is constant in time, which is denoted by Δ. From Eq. (3.18), the phase difference obeys the equation

$$\frac{d\Delta}{dt} = K' \left\{ (2p-1)\Gamma(\tau) + (1-p)\Gamma(\Delta+\tau) + p\Gamma(-\Delta+\tau) \right\}. \tag{3.21}$$

When Δ is constant, we obtain a relation between p and Δ as

$$p = \frac{\Gamma(0) - \Gamma(\Delta)}{2\Gamma(0) - \Gamma(\Delta) - \Gamma(-\Delta)}. \tag{3.22}$$

We designate a two-cluster state satisfying Eq. (3.22) as (p, Δ). The eigenvalues of the stability matrix are calculated as

$$\lambda_1 = K'\{p\Gamma'(\tau) + (1-p)\Gamma'(\Delta+\tau)\}, \tag{3.23}$$

$$\lambda_2 = K'\{(1-p)\Gamma'(\tau) + p\Gamma'(-\Delta+\tau)\}, \tag{3.24}$$

$$\lambda_3 = K'\{(1-p)\Gamma'(\Delta+\tau) + p\Gamma'(-\Delta+\tau)\}, \tag{3.25}$$

where $\Gamma'(x)$ means $(d/dx)\Gamma(x)$. The multiplicities of λ_1, λ_2 and λ_3 are $Np-1$,$N(1-p)-1$ and 1, respectively. λ_1 and λ_2 correspond to fluctuations in phase of the two oscillators inside the phase-advanced and phase-retarded cluster, respectively. λ_3 corresponds to fluctuations in the phase difference Δ between the clusters. Note that there always exists the trivial solution $\Delta = 0$ corresponding to the state of perfect synchrony, and its eigenvalue is $K'\Gamma(\tau)$ with $N-1$ multiplicity.

Substituting Eq. (3.15) into Eq. (3.22), we obtain a relation between p and Δ, the corresponding curve being shown in Fig. 3.3(a). By using this relation, the eigenvalues of (p, Δ) can be obtained, which are displayed in Fig. 3.3(b) as a function of Δ. It is found that any two-cluster states (including the state of perfect synchrony given by $\Delta = 0$) are unstable, and there is a set of (p, Δ) for which $\lambda_1 > 0$ and $\lambda_2, \lambda_3 < 0$. Positive λ_1 means that the two-cluster state is unstable with respect to perturbations inside a phase-advanced cluster. On the other hand, negative λ_2 and λ_3 mean that it is *stable* against perturbations inside a phase-retarded cluster as far as the perfect phase-synchrony of the phase-advanced cluster is maintained. Within a certain range of p, there are pairs of two-cluster states represented by (p, Δ) and (p, Δ') with the same stability property, as they appear as the solid lines in Fig 3.3(a). In the next section, we explain how a *heteroclinic loop* between (p, Δ) and (p, Δ') is persistently formed in our model.

Similarly to the discussion in §3.5, the stability property mentioned above can also be understood in terms of the original model. Every neuron inside the phase-advanced cluster almost always receives pulses when its membrane potential is increasing. Then, the phase-difference between two neurons inside the cluster, if any, almost always increases, so that the phase-advanced cluster is inevitably unstable. On the other hand, the neurons inside the phase-retarded cluster can receive pulses (that was emitted by the phase-advanced cluster) during their resetting. Then, the phase-differences between neurons inside the phase-retarded cluster, if any, become smaller, so that the phase-retarded cluster can be stable.

3.7 Heteroclinic loop

We first note that there is a particular symmetry of our model which turns out crucial to the persistent formation of the heteroclinic loop. The symmetry is given by

$$\left.\frac{d}{dt}\{v_i(t) - v_j(t)\}\right|_{v_i(t)=v_j(t)} = 0 \quad \text{for any } i \text{ and } j. \tag{3.26}$$

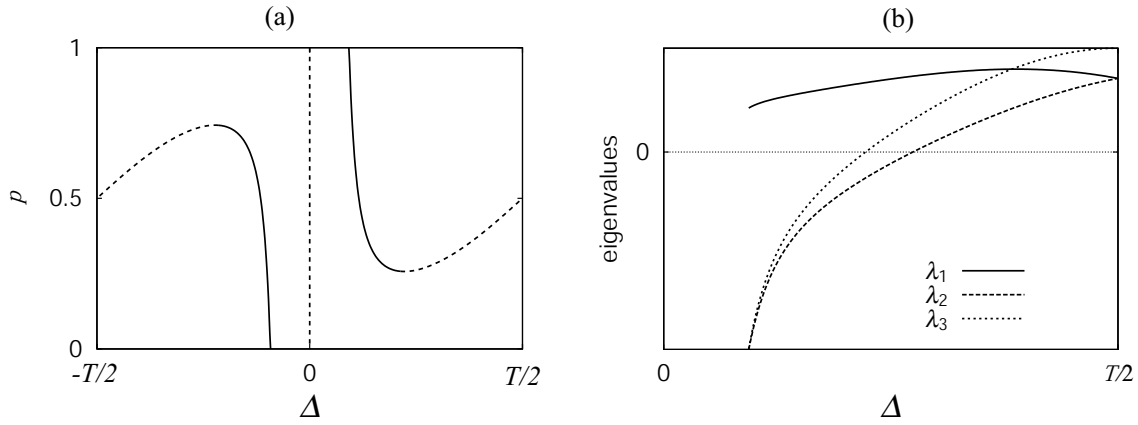

Figure 3.3: (a)Relation between p and Δ associated with two-cluster states. (b)Eigenvalues of two-cluster states as a function of Δ. In (a), the solid and broken lines correspond to the two-cluster state of negative and positive λ_3, respectively. The parameter values are $a = 1.05$ $(T \simeq 3.0), b > a, \alpha^{-1} = 0.3, \beta \to \alpha$ and $\tau = 0.1$. Variation of the parameter values do not change the results qualitatively provided the time constants α^{-1}, β^{-1} and τ are small compared with T.

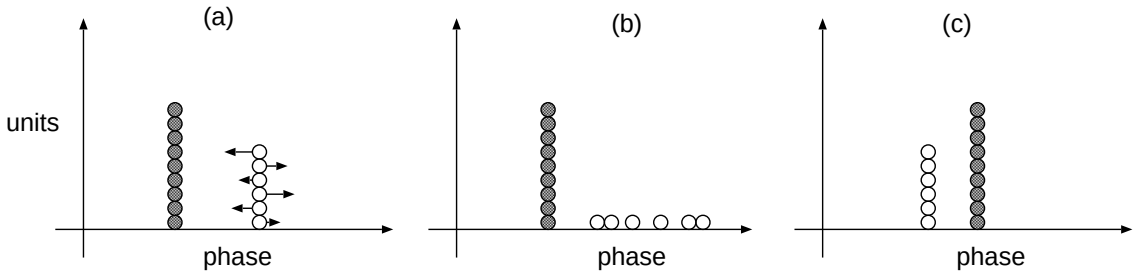

Figure 3.4: Schematic representation of a saddle connection between a pair of two cluster states, starting with the two-cluster state A (a) ending up with the other two-cluster state B (c).

Due to this symmetry, the units which have the same membrane potential at a given time behave identically thereafter. In other words, once a point cluster is formed, it remains a point cluster forever.

We assume that a pair of two-cluster states (called A and B) exists and has the same stability property as that discussed in §3.6, i.e., the phase-advanced cluster is unstable, and the phase-retarded clusters is stable. Suppose that our system is in a two-cluster state A initially. When the oscillators inside the phase-advanced cluster are perturbed while the phase-retarded cluster is kept unperturbed (see Fig. 3.4(a)), the former begins to disintegrate while the latter remains a point cluster. Then, a group of dispersed oscillators and the point cluster coexist in the system (see Fig. 3.4(b)). We know, however, that in the presence of a point cluster, there exist a stable two-cluster state in which the existing point cluster is phase-advanced. From this fact, the dispersed oscillators are expected to converge to form a point cluster coming behind the preexisting point cluster. In this way, the system relaxes to another two-cluster state B (see Fig. 3.4(c)). From the above statement, it is implied that in our high-dimensional phase space there exists a saddle connection from the state A to the state B. The existence of a saddle connection from the state B to the state A can be argued similarly. A heteroclinic loop is thus formed between the pair of the two cluster states A and B.

In terms of the phase model, the above argument can be reinterpreted in a little more precise language. In the phase model given by Eq. (3.18), a symmetry property similar to Eq. (3.26) also holds:

$$\frac{d}{dt}\{\psi_i(t) - \psi_j(t)\}\Big|_{\psi_i(t)=\psi_j(t)} = 0 \quad \text{for any } i \text{ and } j. \tag{3.27}$$

Our argument will be based on the following assumptions:

(a) (p, Δ) with $\lambda_1 > 0$ and $\lambda_2, \lambda_3 < 0$ exits,

(b) (p, Δ') with $\lambda'_2 > 0$ and $\lambda'_1, \lambda'_3 < 0$ exits,

where we define $\Delta > 0$ and $\Delta' < 0$; λ_i and λ'_i $(i = 1, 2, 3)$ are the eigenvalues of (p, Δ) and (p, Δ'), respectively. Note that if $p = 0.5$, the two clusters in question are identical, or $\Delta' = -\Delta$, so that (a) and (b) are identical. Figure 3.5 illustrates a schematic presentation of the $N - 1$ dimensional phase space structure (where we ignore the degree of freedom of the mean phase). E_a and E_r denote the subspaces where the phase-advanced and phase-retarded clusters of (p, Δ) remain point clusters, respectively. By considering the direction of eigenvectors, one can easily confirm that E_a and E_r are identical with the stable subspaces of (p, Δ) and (p, Δ'), respectively. Furthermore, because E_a and E_r are *invariant* subspaces due to the symmetry given by Eq. (3.27), (p, Δ) and (p, Δ') are attractors within E_a and E_r, respectively. Thus, on the assumption that

(c) each attractor is within the basin of attraction of the other attractor,

a heteroclinic loop between (p, Δ) and (p, Δ') is formed.

The saddle connections are *stably* formed through the invariant subspaces that exist for the symmetry of equations of motion, or Eq. (3.26). The heteroclinic loop is thus robust under small perturbations unless the symmetry of Eq. (3.26) is broken. The physical mechanism of the formation of the heteroclinic loop we describe here does not depend on the nature of elements (phase oscillator, limit cycle oscillator, excitable elements, chaotic elements, etc.) and the origin of couplings (diffusive coupling, synaptic coupling, delayed coupling, etc.). It is expected, therefore, that the heteroclinic loop is formed in wide class of population models. We actually find that it arises in a population of coupled limit-cycle oscillators, which is demonstrated in Chap. 4.

Whether the resulting heteroclinic loop is attracting or not depends on the following quantity:

$$\gamma \equiv \frac{\lambda_2 \lambda_1'}{\lambda_1 \lambda_2'}. \tag{3.28}$$

It was argued in Ref. [13] that if $\gamma > 1$, the system approaches the heteroclinic loop and comes to move along it. In that case, the time interval during which the system is trapped near one of the two-cluster states increases exponentially with time. Substituting the eigenvalues obtained from Eqs. (3.23) and (3.24) using Eq. (3.15) into Eq. (3.28), we find that the heteroclinic loops within a certain range of p are in fact attracting for small α^{-1}, β^{-1} and τ. We thus conclude that the slow switching phenomenon discussed in §3.3 results from the existence of an attracting heteroclinic loop.

A phase diagram of the heteroclinic loops and symmetric multi-cluster states is shown in Fig. 3.6, where we choose τ as a control parameter (see Appendix A for the stability analysis of the symmetric multi-cluster states). We have checked that the phase diagram obtained is in good agreement with results obtained by numerical integrations of Eq. (3.1) when K is sufficiently small.

3.8 Conclusion

In this chapter, we have discussed the slow switching phenomenon in a population of delayed pulse-coupled oscillators. We found that the phenomenon is caused by the formation of a heteroclinic loop between a pair of two-cluster states. A particular stability property of the two-cluster states and a certain symmetry of our model are responsible for its formation. Our original model given by Eq. (3.1) is reduced to the standard phase model in the weak coupling limit, by which we succeeded in studying the stability of various cluster states analytically, and confirming the structure of the heteroclinic loop.

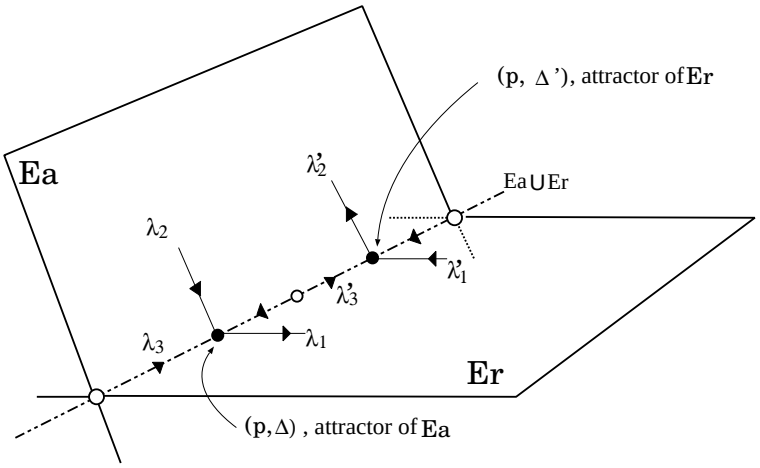

Figure 3.5: Schematic representation of the structure of a heteroclinic loop. (p, Δ) and (p, Δ') become attractors within the invariant subspaces E_a and E_r, respectively.

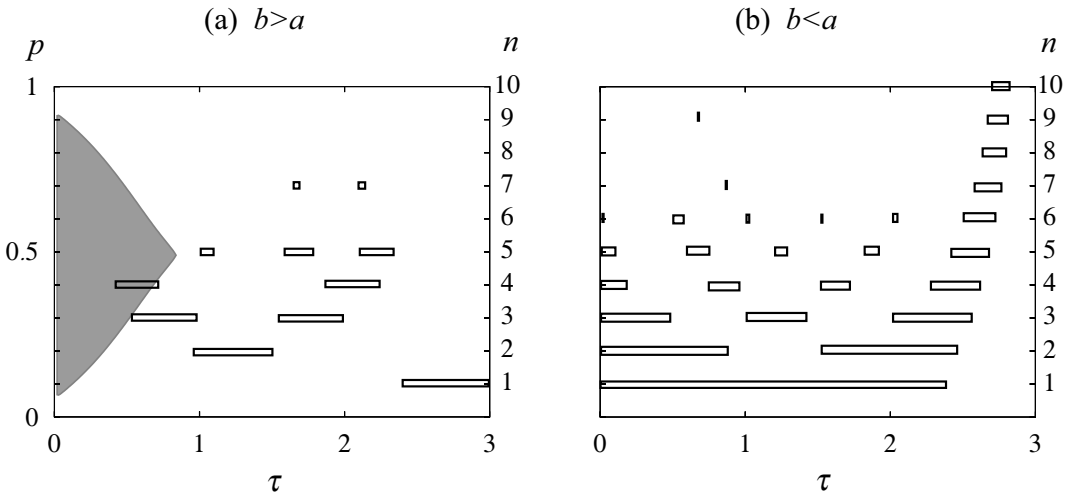

Figure 3.6: Phase diagram of cluster states obtained in the weak coupling limit, where τ is chosen as a control parameter. The parameter values are the same as in Fig. 3.1 with (a)$b > a$ and (b)$b < a$. For given p and τ inside the gray region, γ is larger than one, i.e., the heteroclinic loop between (p, Δ) and (p, Δ') is attracting. Each rectangle placed at n indicates the region of τ within which the symmetric n-cluster state is stable. In (b), there are stable symmetric n-cluster state for $n > 10$ (not shown).

Chapter 4

Coupled Limit-cycle Oscillators and Its Bifurcation Structure

4.1 Introduction

In this chapter, the slow switching phenomenon is discussed in three specific models. Each model has different property in coupling; the first one is a general coupling (i.e., the system obeys ordinary differential equations), the second one is a delayed coupling, and the last one is (delayed) pulse coupling. In the latter two models, it is shown that time delay in coupling plays a essential role in the formation of heteroclinic loops. In particular, we will argue that the stability condition for the formation of the heteroclinic loop is easily satisfied near the bifurcation where the state of perfect synchrony loses stability. Through the discussion in this chapter, one may understand the slow switching phenomenon occurs in a wide class of globally coupled oscillators.

4.2 Hindmarsh-Rose oscillators coupled by gap junctions

We consider a general model of globally coupled identical oscillators with the form:

$$\frac{d}{dt}\boldsymbol{X}_i(t) = \boldsymbol{F}(\boldsymbol{X}_i) + \frac{K}{N}\sum_{j=1}^{N}\boldsymbol{G}(\boldsymbol{X}_i, \boldsymbol{X}_j), \tag{4.1}$$

Here $\boldsymbol{X}_i, \boldsymbol{F}$ and $\boldsymbol{G}$ are m-dimensional real vectors ; and K is a positive constant. In Eq. (4.1), a symmetry property similar to Eq. (3.26) or Eq. (3.27) also holds, which is represented as

$$\frac{d}{dt}\{\boldsymbol{X}_i(t) - \boldsymbol{X}_j(t)\}\Big|_{\boldsymbol{X}_i(t)=\boldsymbol{X}_j(t)} = 0 \qquad \text{for all} \quad i \text{ and } j. \tag{4.2}$$

Note that all the models introduced in this chapter possess the similar symmetric property, so that once a point cluster is formed in the system, it remains a point cluster forever.

Suppose that the local dynamics is two-dimensional, i.e. $\boldsymbol{X} = (x, y)$, and the specific forms of $\boldsymbol{F}$ and $\boldsymbol{G}$ are given by

$$\boldsymbol{F}(\boldsymbol{X}_i) = \begin{pmatrix} F_x \\ F_y \end{pmatrix} = \begin{pmatrix} 3{x_i}^2 - {x_i}^3 + y_i - \mu \\ 1 - 5{x_i}^2 - y_i \end{pmatrix}, \tag{4.3}$$

$$\boldsymbol{G}(\boldsymbol{X}_i, \boldsymbol{X}_j) = \begin{pmatrix} G_x \\ G_y \end{pmatrix} = \begin{pmatrix} x_j - x_i \\ 0 \end{pmatrix}, \tag{4.4}$$

The corresponding equation $\dot{\boldsymbol{X}} = \boldsymbol{F}$ is called the Hindmarsh-Rose model which was originally proposed for a neural oscillator [20]. Each elements becomes a limit-cycle oscillator if $-11.5 < \mu < 0.8$ [21]. We set $\mu = -1$, which gives the intrinsic period $T \simeq 6.2$. The coupling given by Eq. (4.4) is called a diffusive coupling, and in terms of neurophysiology, this corresponds to the electrical synapse formed by gap junctions [22].

In the model given above, the slow switching phenomenon is generally obtained for small K. Some numerical results obtained with $K = 0.1$ and $N = 100$ under random initial conditions are summarized as follows. In each trial of numerical integration, the system converges after a long transient to a two-cluster state which is periodic in time. Figure 4.1 displays a time series of the order parameter. Before the convergence, we can see that the system repeats switching back and force between a pair of two-cluster states. Relative population of the clusters is generally depends on the initial condition. If we give very small perturbations independently to the oscillators in a two-cluster state after the convergence, the clusters start to disintegrate, implying its linear instability. Thus, an attracting heteroclinic loop between a pair of two-cluster states should exist.

4.3 Stability analysis

We can perform the stability analysis of the two-cluster states through the method of the *phase reduction*. In general, coupled oscillators is reduced to the phase model when the coupling is sufficiently weak [6]. There is a general formula to derive an evolution equation for phases of the oscillators. For the model given by Eq. (4.1), the corresponding phase dynamics reads

$$\frac{d}{dt}\psi_i(t) = 1 + \frac{K}{N}\sum_{j=1}^{N}\Gamma(\psi_i - \psi_j), \tag{4.5}$$

where ψ_i is the phase of the i-th oscillator which varies between 0 and the intrinsic period T, and Γ is the coupling function which is T-periodic. Roughly speaking, ψ_i is defined so as to have a constant velocity along a limit-cycle in the one-oscillator phase space when $K = 0$. The coupling function is computed numerically for specific F and G given by Eqs. (4.3) and (4.4), which is displayed in Fig. 4.2. One should notice that the similarity between Fig. 4.2 and Fig. 3.1. The existence and stability analysis are performed similarly to §3.6, which shows that the stability property of the two-cluster states admit, based on the argument in §3.7, the existence of attracting heteroclinic loops within a certain range of p.

When K becomes too large, such as $O(1)$, the two-cluster states gives way to the state of perfect synchrony by which the heteroclinic loop disappears. It seems that the heteroclinic loop does not persist when the coupling is so strong that the phase description completely breaks down.

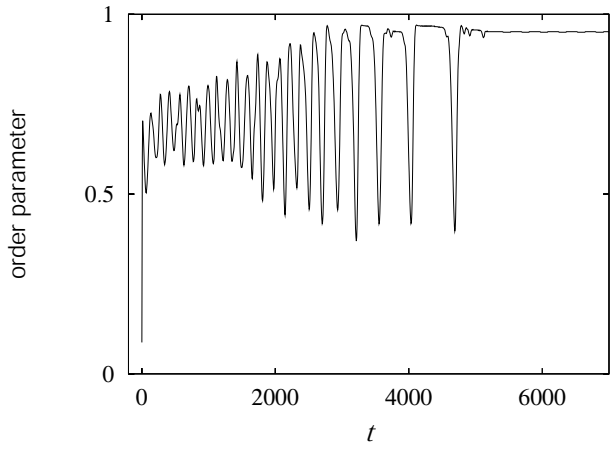

Figure 4.1: Time series of the order parameter. The order parameter O is conveniently defined in the following way. Let t_j $(j = 0, 1, 2, \cdots)$ denote the time at which the representative point of the j-th oscillator crosses a given section Σ in the 1-oscillator phase space. The order parameter at time $t = t_N$ is defined as $O(t = t_N) = \frac{1}{N}\left|\sum_{j=1}^{N} \exp\left[i\frac{2\pi(t_j - t_0)}{t_N - t_0}\right]\right|$ as a generalization of Eq. (3). Since the oscillators cross Σ again and again, the order parameter at discrete times $t = t_{kN}$ $(k = 1, 2, \cdots)$ can be defined similarly. Note that $O(t) = 1$ when the oscillators are perfectly synchronized and $O(t) = 0$ when their phases are uniformly distributed.

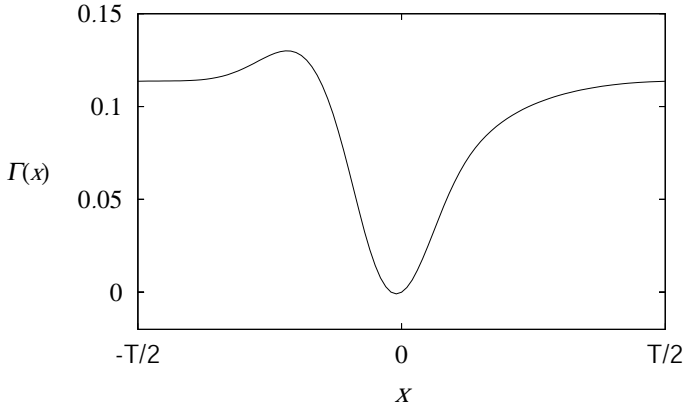

Figure 4.2: Coupling function of the reduced model. The minimum of $\Gamma(x)$ appears at a negative x. $T \simeq 6.2$ in the figure.

4.4 Hindmarsh-Rose oscillators with delayed coupling

It is well known that the state of perfect synchrony, i.e. all the oscillators have an identical phase, is often obtained in globally coupled identical oscillators. For example, it is generally stable for arbitrary coupling strengths with the following form of coupling:

$$\boldsymbol{G}(\boldsymbol{X}_i, \boldsymbol{X}_j) = \boldsymbol{X}_j(t) - \boldsymbol{X}_i(t). \tag{4.6}$$

We show in this section that time delay introduced into coupling causes instability of the state of perfect synchrony, which at the same time is accompanied by the appearance of the heteroclinic loop. We again assume F as Eq. (4.3), and G as a uniformly delayed coupling, given by

$$\boldsymbol{G}(\boldsymbol{X}_i, \boldsymbol{X}_j) = \boldsymbol{X}_j(t-\tau) - \boldsymbol{X}_i(t) \tag{4.7}$$

where τ denotes delay. Note that the symmetry property (4.2) still holds when the coupling involves a uniform delay. We will show some numerical results with the same parameter values as in §4.2. Figure 4.3 displays a time trace of the order parameter. Without delay, the system under various initial conditions immediately converges to the state of perfect synchrony. As τ is increased, the one-cluster state persists up to a critical value τ_0 beyond which the cluster splits into two and at the same time heteroclinic loops are formed. In the parameter values given above, this critical value seems to be about 0.18.

The phase reduction of the model, which is applicable when the coupling is weak, provides a clear understanding of the above result. For a system with a uniformly delayed coupling such as Eq. (4.7), the corresponding reduced model takes the form

$$\frac{d}{dt}\psi_i(t) = 1 + \frac{K}{N}\sum_{j=1}^{N}\Gamma\big(\psi_i(t) - \psi_j(t-\tau)\big). \tag{4.8}$$

Since the second term on the right-hand side is much smaller than the first term by assumption, (4.8) is further reduced to the form

$$\frac{d}{dt}\psi_i(t) = 1 + \frac{K}{N}\sum_{j=1}^{N}\Gamma\big(\psi_i(t) - \psi_j(t) + \tau\big). \tag{4.9}$$

Thus, there is no explicit delay in coupling, while its effect has now been converted to a phase shift of the coupling function by τ, as illustrated in Fig. 4.4. The stability of the state of perfect synchrony depends entirely on the sign of $\Gamma'(\tau)$ (see §3.6), so that the state is stable for small τ. As τ increases, it becomes less stable, and at $\tau > \tau_c$ it becomes unstable, where τ_c is defined as the value of τ which minimizes $\Gamma(\tau)$ (see Fig. 4.4). Note that the ciritical value τ_0 which was obtained through numerical simulations is expected to agree with τ_c when the coupling is sufficiently weak. For $\tau > \tau_c$, the coupling function

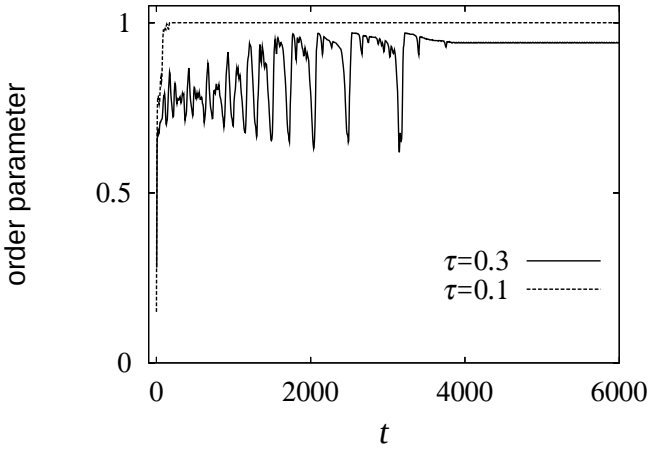

Figure 4.3: Time series of the order parameter. The definition of the order parameter is the same as in Fig. 4.1. For $\tau < \tau_0$, the system shows perfect synchrony. On the other hand, for $\tau > \tau_0$ the slow switching phenomenon arises. The critical value τ_0, which is evaluated by numerical simulations, is about 0.18.

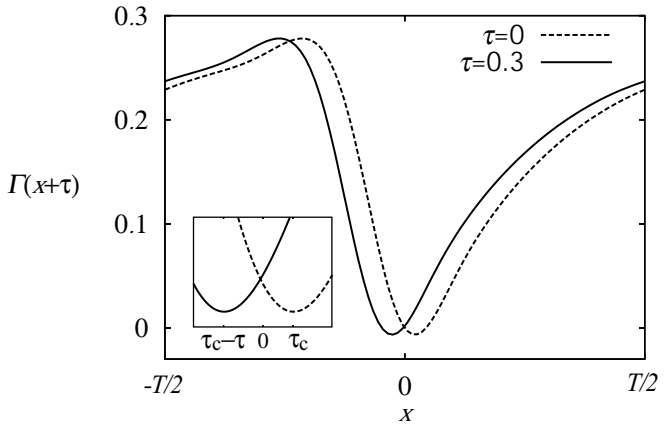

Figure 4.4: Coupling functions. The dotted line is obtained numerically from (4.1) with (4.3) and (4.6), while the solid line is obtained just by a phase shift of dotted line by $-\tau$. The effect of the delay is equivalent to a simple modification of the coupling function in the weak-coupling limit. $T \simeq 6.2$ and $\tau_c \simeq 0.13$ in the figure.

assumes a similar shape to Fig. 3.1 and Fig. 4.2. We have checked by using this coupling function that the stability of the two-cluster states within a certain range of p admits the existence of attracting heteroclinic loops for $\tau > \tau_c$.

This transition occurs through a pitchfork bifurcation at $p = 0.5$ and a transcritical bifurcation at $p \neq 0.5$. In a two-cluster state (p, Δ) (the definition of (p, Δ) is given in §3.6), the phase difference Δ obeys the equation

$$\frac{d\Delta}{dt} = K\left\{(2p-1)\Gamma(\tau) + (1-p)\Gamma(\Delta+\tau) + p\Gamma(-\Delta+\tau)\right\}. \tag{4.10}$$

Using $\Gamma(x)$ readed out from Fig. 4.4, we obtain bifucation diagrams for given p, which is shown in Fig. 4.5. The solid and broken lines correspond to steady solutions with negative and positive λ_3, respectively. We can see that the state of perfect synchrony ($\Delta = 0$) loses stability at $\tau = \tau_c$, and a pair of two solid branches arises for $\tau > \tau_c$. Evaluating the eigenvalues λ_1 and λ_2 of the solid branches, we confirm that an attracting heteroclinic loop can be formed between these two brances within a certain range of p. The detailed analyses near the bifucation point will be given in §4.6.

4.5 Morris-Lecar oscillators with delayed pulse-coupling

The final example is exhibited by a population of neural oscillators. Each neurons obeys the following evolutional equations called the Morris-Leccar model, given by

$$C\frac{dv_i}{dt} = -\bar{g}_{\mathrm{Ca}} m_\infty(v_i)(v_i - V_{\mathrm{Ca}}) - \bar{g}_{\mathrm{K}} w_i (v_i - V_{\mathrm{K}}) - \bar{g}_{\mathrm{L}}(v_i - V_{\mathrm{L}}) + I_i, \tag{4.11}$$

$$\frac{dw_i}{dt} = \phi\frac{[w_\infty(v_i) - w_i]}{\tau_w(v_i)}, \tag{4.12}$$

with

$$m_\infty(v_i) = 0.5[1 + \tanh\{(v_i - V_1)/V_2\}], \tag{4.13}$$

$$w_\infty(v_i) = 0.5[1 + \tanh\{(v_i - V_3)/V_4\}], \tag{4.14}$$

and

$$\tau_w(v_i) = 1/\cosh\{(v_i - V_3)/(2V_4)\}, \tag{4.15}$$

where v_i is the membrane potential, w_i is the fraction of potassium channel open at t, and I_i is the external current injected into the nueron. The Morris-Lecar model is a two-variable version of the Hodgikin-Huxlex type model, which has been extensively studied in Ref. [23]. The parameter values follow Ref. [23], given by $V_1 = -1.2$, $V_2 = 18$, $V_3 = 12$, $V_4 = 17.4$, $\bar{g}_{\mathrm{Ca}} = 4.0$, $\bar{g}_{\mathrm{K}} = 8.0$, $\bar{g}_{\mathrm{L}} = 2$, $V_{\mathrm{Ca}} = 120$, $V_{\mathrm{K}} = -84$, $V_{\mathrm{L}} = -60$, $C = 20\mu\mathrm{F/cm}^2$

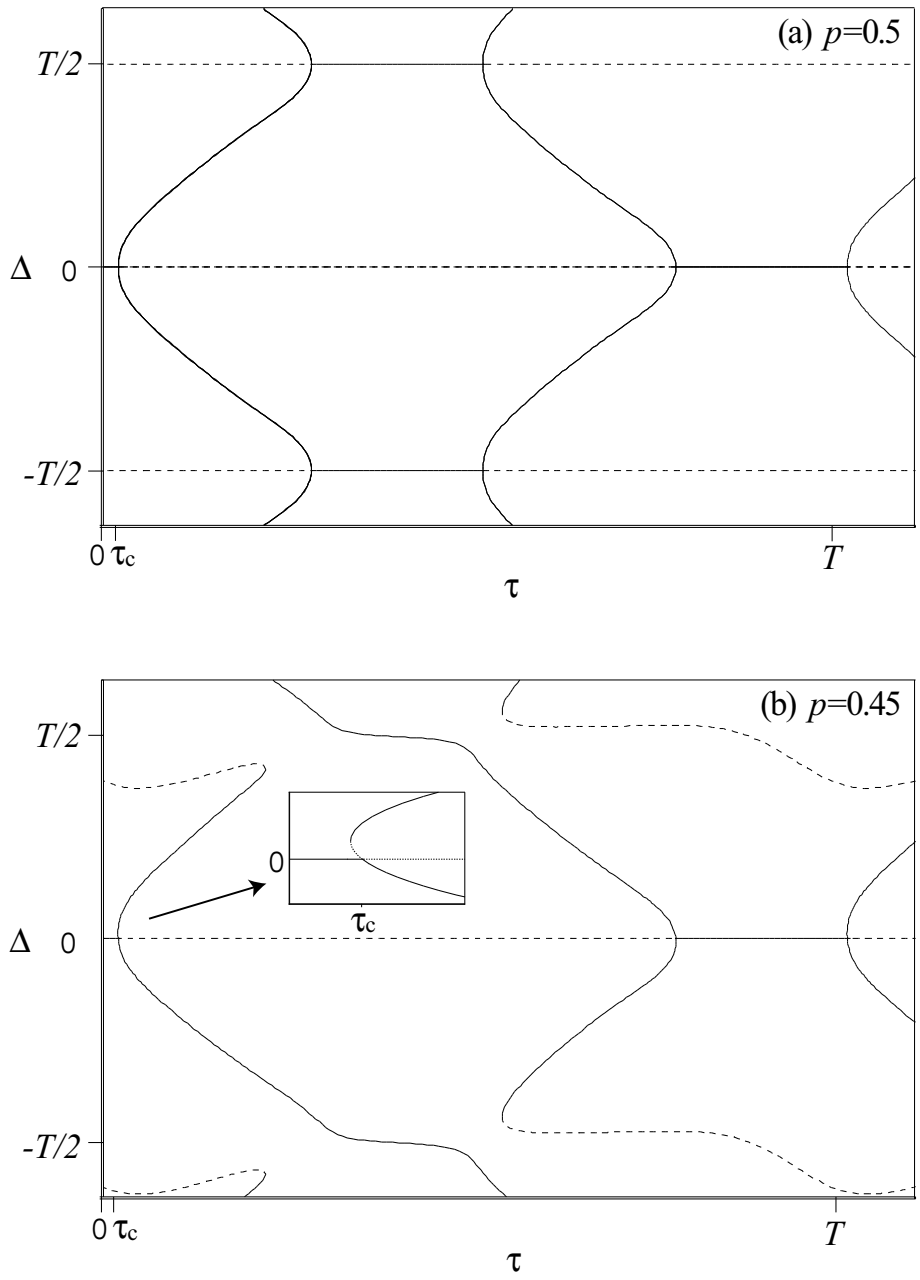

Figure 4.5: Bifucation diagrams for (a)$p = 0.5$ and (b)$p = 0.45$. $T \simeq 6.2$ and $\tau_c \simeq 0.13$ in the figure.

and $\phi = 1/15$. The basic properties of this model for constant I_i are as follows. For $0 \leq I_i \leq I_{\rm a}$, the system has one stable fixed point in the one-oscillator phase plane. Thus, v converges to a cirtain value, so-called the resting potential. In this range of the current, the system is excitable. This fixed point becomes unstable at $I_i = I_{\rm a}$ via a saddle-node bifucation and a stable limit cycle then appears by homoclinic connection. The onset of the periodic motion associated with this limit cycle begins at zoro frequency, which is a typical property of homoclinic connection. The system is monostable up to $I_i = I_{\rm b}$ at which the subcritical Hopf bifurcation occurs. For the parameter values ginve above, $I_{\rm a}$ and $I_{\rm b}$ is about 40 and 98 respectively.

We assume the external current input I_i as the following form:

$$I_i = I + \frac{K}{N}(V_{\rm rev} - v_i)E(t), \tag{4.16}$$

where I is a constant current input, $V_{\rm rev}$ is a constant denoting reversal potential, and $E(t)$ is the same global variable as Eq. (3.2). A series of times at which the j-th neuron spikes is defined by

$$V_j(t_j^{\rm spikes}) = V_{\rm th} \quad \text{and} \quad \frac{dv_j}{dt} > 0. \tag{4.17}$$

Neumerical results obtained with $I = 44$ (which corresponds to the intrinsic period $T \simeq 109$), $K = 0.1, N = 100, \alpha = 3.5, \beta \to \alpha, V_{\rm rev} = 100$ and $V_{\rm th} = 0$ are summarized as follows. For small τ, the system generally shows pefect synchrony. Around $\tau = 2$, we can obtain two-cluster states involving slow switching as well as the state of perfect synchrony, and their appearance depends on initial conditions. Such two-cluster states seems to vanish around $\tau = 4$, and steady multi-cluster states begin to arise instead. The state of perfect synchony remains stable up to about $\tau = 4.5$ beyound which the steady multi-cluster states generally arise.

Similarly to the preceding sections, the phase reduction of the model provides a clear understanding of the results given above. The coupling funtion for the model under consideration is obtained numerically, which is exhibited in Fig. 4.6. Using this coupling function, we obtain bifucation diagrams of the two-cluster states for given p, which are illustrated in Fig. 4.7. We can see that a pair of two-cluster state with negative λ_3 exist not only for $\tau > \tau_{\rm c}$ but also for $\tau < \tau_{\rm c}$. We checked that the stability of the branches actually admits the existence of an attrating heteroclinic loop. Thus, both the state of perfect synchrony and the heteroclinic loops are stable over some region of $\tau < \tau_{\rm c}$. This bistability comes from a particular phase dynamics near the bifucation point, which differs from that in §4.4. We will explain it in the next section.

Similar results can be obtained if we increase α^{-1} instead of τ, which implies that the delay of the coupling effectively increases with α^{-1}. This can be seen visually in

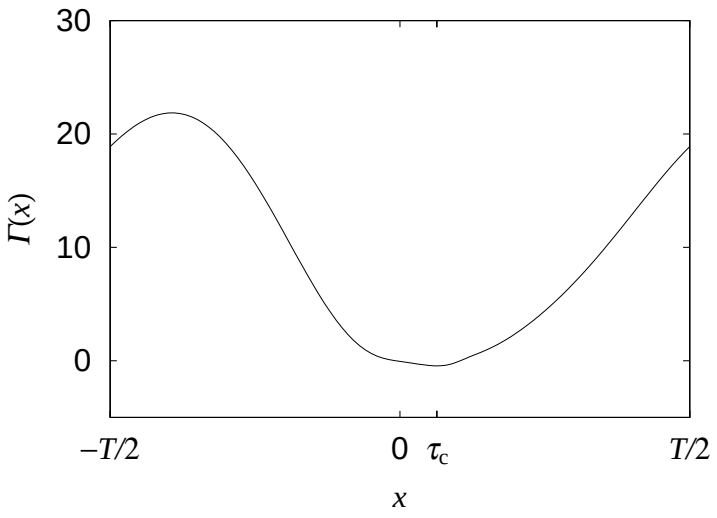

Figure 4.6: Coupling function.$T \simeq 109$ and $\tau_c \simeq 6.4$.

Fig. 4.6, from which we find that the coupling function is further shifted to left for larger α^{-1}. Such an effect of α^{-1} is intuitively understood from the nature of the pulse function given by Eq. (3.3), i.e., it takes the time of α^{-1} to rise the pulse, so that the coupling is effectively delayed. The similar effect exists in the case of LIF as well (see Fig. 3.1). $Z(x)$ is identical with the coupling function in the limit $\alpha^{-1} \to 0$, and the coupling function $\Gamma(x)$ is effectively sifted to left compared by Z. One can check that the coupling function is shifted further to left for larger α^{-1}. The minimum of the coupling function, however, is little shifted due to the sudden drop of $Z(x)$.

4.6 Near the bifucation point

In this section, we concentrate on the vicinity of the bifurcation point where the state of perfect synchrony loses stability. Although we can say nothing about the global structure of the phase space in the argument here, we show the local stability property necessary for the existence of an attracting heteroclinic loop, which was aruged in §3.7, is easily satisfied near the bifurcation point. The model equation we consider is Eq. (4.9), given by

$$\frac{d}{dt}\psi_i(t) = 1 + \frac{K}{N}\sum_{j=1}^{N}\Gamma\big(\psi_i(t) - \psi_j(t) + \tau\big), \tag{4.18}$$

where we treat τ as a control parameter. We assume that the coupling function $\Gamma(x)$ is minimum at $x = \tau_c$. Then, for small $\tilde{x} \equiv x - \tau_c$, we may expand Γ as

$$\Gamma(x) = c_0 + c_2\tilde{x}^2 - c_3\tilde{x}^3 + O(\tilde{x}^4), \tag{4.19}$$

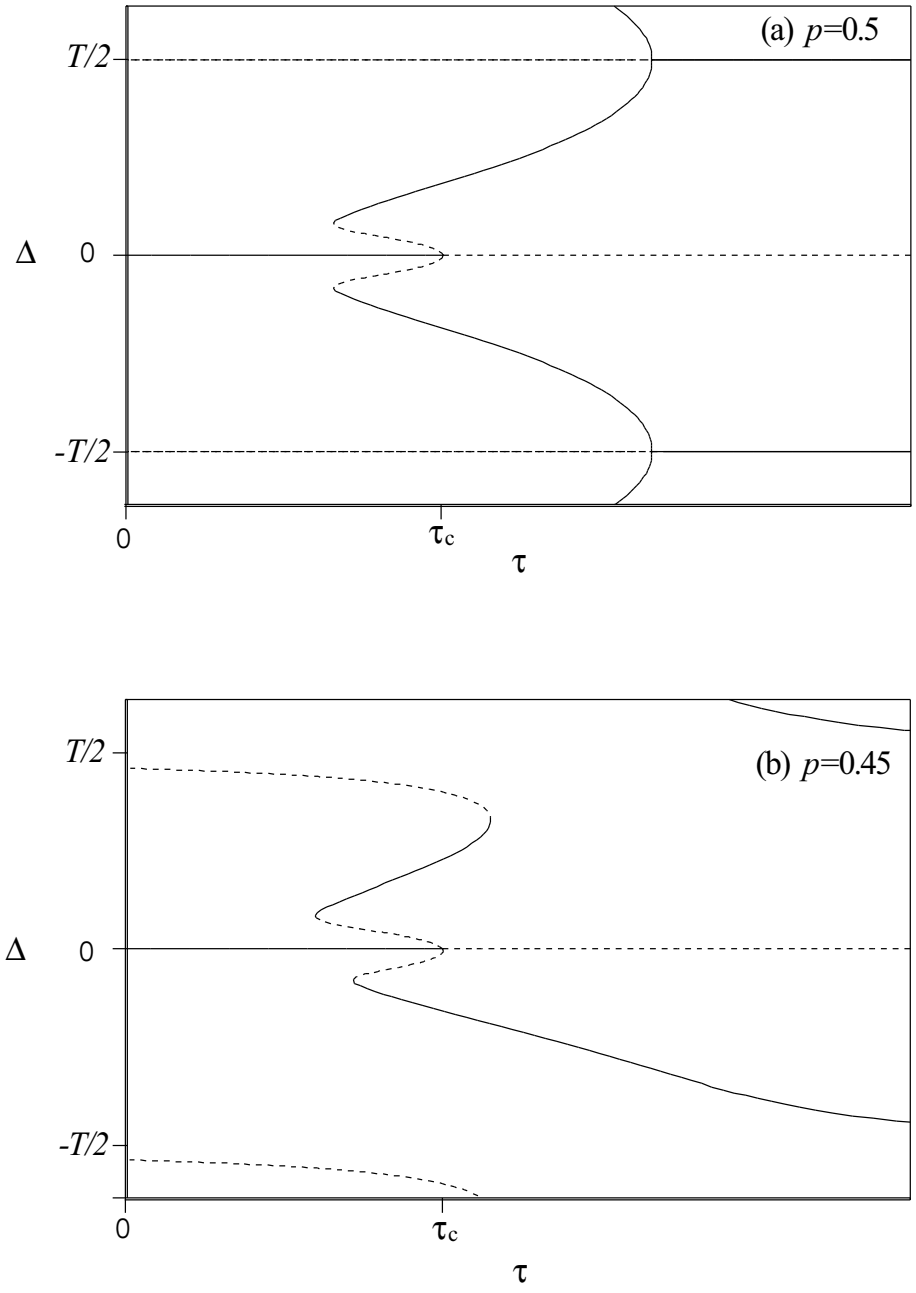

Figure 4.7: Bifucation diagrams for (a)$p = 0.5$ and (b)$p = 0.45$. $T \simeq 109$ and $\tau_c \simeq 6.4$.

where c_2 is positive. Suppose that c_3 is positive, which is actually the case for the coupling function displyed in Fig. 4.2. In this case, heteroclini loops arises *supercritically*. We put $c_0 = 0$ and $c_3 = 1$ by properly rescaling K and shifting the natural frequency in Eq. (4.18). In order to find possible two-cluster states, we solve Eq. (3.22) using Eq. (4.19). We then obtain three solutions for Δ as a function of p and τ. One is the trivial solution $\Delta = 0$ (the perfect synchrony), and the others are given by

$$\Delta = \frac{(1-2p)(c_2 - 3\tilde{\tau})}{2} \pm \sqrt{\frac{(1-2p)^2(c_2-3\tilde{\tau})^2}{4} + 2c_2\tilde{\tau}}, \tag{4.20}$$

where $\tilde{\tau} \equiv \tau - \tau_c$. Note that the expression above using the approximate Γ given by Eq. (4.19) is valid only for small Δ, which is actually the case if p is close to $1/2$ and $\tilde{\tau}$ is small. Substituting Eq. (4.20) into Eqs. (3.23)-(3.25), we obtain eigenvalues associated with the two-cluster states. The resulting bifurcation diagram for given p is shown in Fig. 4.9. The solid and broken lines give the branches of negative and positive λ_3, respectively. Two solid branches exist for $\tau > 0$, which are represented by (p, Δ) and (p, Δ') with $\Delta > 0$ and $\Delta' < 0$. One can easily comfirm that the eigenvalues of these states satisfy $\lambda_1, \lambda_2' > 0$ and $\lambda_2, \lambda_3, \lambda_1', \lambda_3' < 0$ for arbitrary p and small $\tilde{\tau}$. The quantity γ defined by Eq. (3.28) can also be calculated and turns out to be larger than 1. Thus, all the local stability conditions for the existence of an attracting heteroclinic loop are generally satisfied just above the bifurcation point provided $c_3 > 0$.

It is also possible that a heteroclinic loop is formed when $c_3 < 0$. In that case, it is expected to arise *subcritically*, so that both the heteroclinic loop and the state of perfect synchrony may coexist over some region of negative τ. We have found that such bistability actually arises in the model introduced in §4.5. The expansion of the coupling function displayed in Fig. 4.6 for small $\tilde{x}$ actually shows that c_3 is negative. We have to consider higher orders to comfirm the bifurcation structure for $c_3 < 0$, which is complicated in general and is not studied further.

4.7 Conclusion

We have shown that the heteroclinic loop arise in three specific models of globally coupled oscillators. In particular, it was argued that time-delay in coupling easily induce bifucation to the formation of the heteroclinic loop. The heteroclinic loop can arise via both supercritical and subcritical bifurcations. In the supercritical one, a pair of two-cluster states arises above the bifurcation point, which always satisfy the local stability condition for the formation of an attracting heteroclinic loop. In the subritical one, a heterocinic loop can arise below the bifurcation point, so that both the state of perfect synchrony and the heteroclinic loop coexist over the some region of the bifurcation parameter.

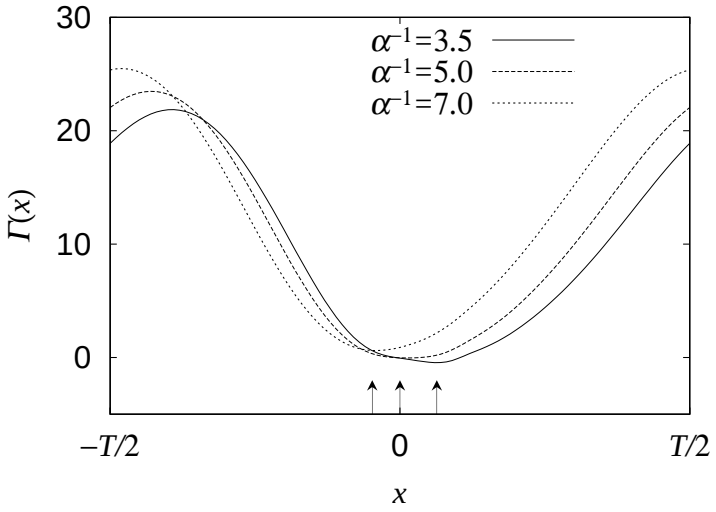

Figure 4.8: Coupling functions. The arrows indicate minimum points of the coupling functions.

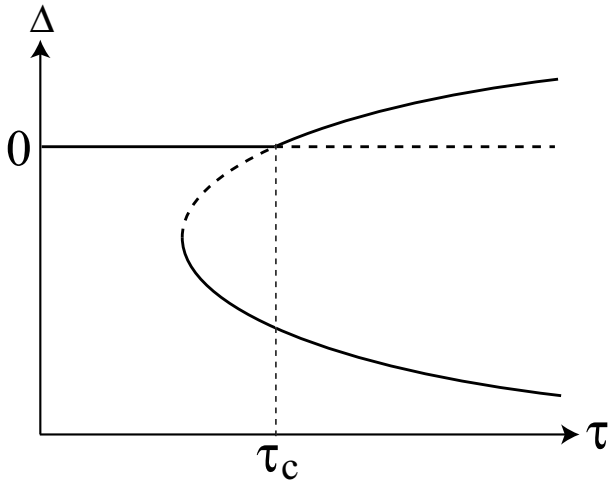

Figure 4.9: Bifurcation diagram around $\tau = \tau_c$ for $p \neq 0.5$. A pair of solid branches exist for $\tau > \tau_c$, which can be connected heteroclinically.

Chapter 5

General Conclusion

In the present thesis, we have discussed the slow switching phenomenon in globally coupled oscillators. The phenomenon appears as a result of approach of the system to heteroclinic loops. A particular stability property of two-cluster states and a certain symmetry of our model are responsible for the formation of the heteroclinic loop. The resulting heteroclinic loop is stably formed through invariant subspaces that exist for the certain symmetry of our model, and it is robust under small perturbation unless the symmetry is broken. It was also argued that time delay in coupling easily causes the transition from the state of the perfect synchrony to the formation of the heteroclinic loop. When the state of prefect synchrony loses statbility supercritically, local stability conditions necessary for this formaion is generally satisfied just above the bifurcation point.

We gained considerable advantages in a theoritical approach by assuming *weak* coupling. In Chap. 3, our model is reduced to a standard phase model that is free from memory effect involved originally. In Chap. 3, we again obtain a phase model by which we can ignore irrelevant degrees of freedom associated with amplitude directions. In the phase model obtained, the effect of delay in coupling is converted a phase shift of the coupling function, which drastically reduces a difficulty in treating delayed coupling. In particular, the bifurcation structure induced by delay can clearly be understood through the phase model obtained.

Acknowledgments

I am very grateful to Prof. Y. Kuramoto for both material and moral support throughout my study. His works and his way of thinking have still exerted a deep influence on me. I like to thank Prof. S. Shinomoto, Dr. T. Mizuguchi and Dr. H. Nakao for broad support and instructive advise. I also thank to Dr. T. Chawanya, Dr. T. Aoyagi, Dr. H. Sakai, Mr. T. Funada, Mr. J. Teramae, Mr. D. Tanaka, and the members of the Theoretical Physics Group of Kyoto University for valuable discussions and precious advice. For a pleasant and relaxed atmosphere in the study room, I am indebted to Ms. F. Hirono, Mr. S. Shima and Ms. Y. Kawaguchi who occupy the same study room. I thank all of my friends for encouraging and inspiring me. I also appreciate an atmosphere of freedom, people, nature, and exercise grounds in Kyoto University and Kyoto City.

I would like to express my deepest gratitude to my parents, my brother and my sisters for their generous support.

Appendix A

Symmetric multi-cluster state

According to Ref. [10], we summarize here the existence and the stability analysis of *symmetric multi-cluster states* in the phase model given by Eq. (3.18), in which each cluster consists of the same number of oscillators. In Eq. (3.18), there always exist symmetric n-cluster states rotating steadily, which can be represented by

$$\psi_i = \Omega_n t + \frac{T(i \bmod n)}{n}, \tag{A.1}$$

where Ω_n is a constant frequency of the symmetric n-cluster state, given by

$$\Omega_n = \omega + \frac{K'}{n} \sum_{k=0}^{n-1} \Gamma\left(\frac{Tk}{n} + \tau\right). \tag{A.2}$$

The eigenvalues associated with them are calculated as

$$\lambda_{\text{intra}} = \frac{K'}{n} \sum_{k=0}^{n-1} \Gamma'\left(\frac{Tk}{n} + \tau\right), \tag{A.3}$$

$$\lambda_{\text{inter}}^{p} = \frac{K'}{n} \sum_{k=0}^{n-1} \Gamma'\left(\frac{Tk}{n} + \tau\right)(1 - \exp[-\mathrm{i}Tkp/n]). \tag{A.4}$$

λ_{intra} is a intra-cluster eigenvalue with multiplicity of $N - n$. $\lambda_{\text{inter}}^{p}$ (p=1,...,n-1) are associated with inter-cluster fluctuations. If all these eigenvalues have negative real part, the symmetric n-cluster state is stable.

Bibliography

[1] A. T. Winfree. Biological rhythms and the behavior of populations of coupled oscillators. *J. Theor. Biol.*, Vol. 16, p. 15, 1967.

[2] A. T. Winfree. *The Geometry of Biological Time.* Springer, New York, 1980.

[3] Leon Glass, Peter Hunter, and Andrew McCulloch, editors. *Theory of Heart.* Springer, Verlag, 1990.

[4] J. Buck. Synchronous rhythmic flashing in fireflies. 2. *Q. Rev. Biol.*, Vol. 63, p. 265, 1988.

[5] A.K. Ghosh, B. Chance, and E.K. Pye. Metabolic coupling and synchronization of nadh oscillations in yeast cell populations. *Arch. Biochem. Biophys.*, Vol. 145, p. 319, 1971.

[6] Y. Kuramoto. *Chemical Oscillation, Waves, and Turbulence.* Springer, New York, 1984.

[7] Steven H. Strogatz and Ian Stewart. Coupled oscillators and biological synchronization. *Scientific American*, Vol. 269, p. 68, 1993.

[8] S. H. Strogatz. Norbert wiener's brain waves. In S. Levin, editor, *Lecture Notes in Biomathematics*, Vol. 10. Springer, New York, 1994.

[9] A. Pikovsky, M. Rosenblum, and J. Kurths. *Synchronization.* Cambridge University Press, 2001.

[10] K. Okuda. Variety and generality of clustering in globally coupled oscillators. *Physica D*, Vol. 63, p. 424, 1993.

[11] Vladimir K. Vanag, et al. Oscillatory cluster patterns in a homogeneous chemical system with global feedback. *Nature*, Vol. 406, p. 389, 2000.

[12] Minseok Kim, et al. Controlling chemical turbulence by global delayed feedback: Pattern formation in catalytic co oxidation on pt(110). *Science*, Vol. 292, p. 1357, 2001.

[13] D. Hansel, G. Mato, and C. Meunier. Clustering and slow switching in globally coupled phase oscillators. *Phys. Rev. E*, Vol. 48, p. 347, 1993.

[14] A. Treisman. The binding problem. *Curr. Opin. Neurobiol.*, Vol. 6, p. 171, 1996.

[15] Alain Destexhe, Zachary F. Mainen, and Terrence J. Sejnowski. Kinetic models of synaptic transmission. In C. Koch and I. Segev, editors, *Method in Neuronal Modeling*, chapter 1. MIT Press, Cambridge, 2nd edition, 1998.

[16] R. E. Mirollo and S. H. Strogatz. Synchronization of pulse-coupled biological oscillators. *SIAM J. Appl. Math.*, Vol. 50, p. 1645, 1990.

[17] Y. Kuramoto. Collective synchronization of pulse-coupled oscillators and excitable units. *Physica D*, Vol. 50, p. 15, 1991.

[18] Y. Sakai, S. Funahashi, and S. Shinomoto. Temporally correlated inputs to leaky integrate-and-fire models can reproduce spiking statics of corical neurons. *Neural Networks*, Vol. 12, p. 1181, 1999.

[19] L. F. Abbott and Cark van Vreeswijk. Asynchronous state in networks of pulse-coupled oscillators. *Phys. Rev. E*, Vol. 48, p. 1483, 1993.

[20] J. L. Hindmarsh and R. M. Rose. A model of neuronal bursting using three coupled first order differential equations. *Proc. R. Soc. London B*, Vol. 221, p. 87, 1984.

[21] S. Raghavachari and J. A. Glazier. *Phys. Rev. Lett.*, Vol. 82, p. 2991, 1999.

[22] Larry Abbott and Eve Marder. Modeling small network. In C. Koch and I. Segev, editors, *Method in Neuronal Modeling*, chapter 10. MIT Press, Cambridge, 2nd edition, 1998.

[23] John Rinzel and Bard Ermantrout. Analysis of neural excitability and oscillations. In C. Koch and I. Segev, editors, *Method in Neuronal Modeling*, chapter 7. MIT Press, Cambridge, 2nd edition, 1998.